INTERNATIONAL JOURNAL OF REFRIGERATION 75 (2017) 117–128

Available online at www.sciencedirect.com

ScienceDirect

journal homepage: www.elsevier.com/locate/ijrefrig

Thermodynamic modelling and parameter determination of ejector for ejection refrigeration systems

*Zhiwei Ma, Huashan Bao *, Anthony Paul Roskilly*

Sir Joseph Swan Centre for Energy Research, Newcastle University, Newcastle upon Tyne NE1 7RU, UK

ARTICLE INFO

Article history:
Received 11 November 2016
Received in revised form 5 December 2016
Accepted 7 December 2016
Available online 13 December 2016

Keywords:
Ejector modelling
Ejector refrigeration
Experimental verification
Parameter determination
Critical operation mode

ABSTRACT

This paper presents a detailed thermodynamic modelling method of an ejector for ejection refrigeration system. In this model, the primary flow in the ejector was assumed to fan out from the nozzle without mixing with the secondary flow in a certain downstream distance, so that a hypothetical throat was formed where the secondary flow reached the sound speed. However, the area of this hypothetical throat remained unknown. Therefore, based on several sets of experimental results, the present study developed empirical correlations of the hypothetical throat area to aid further modelling. The ratio of the hypothetical throat area to the mixing area was correlated with two dimensionless variables: one was the ratio of nozzle throat area to the mixing area, and the other one was the primary and secondary flow pressure ratio. The model has been validated by the measured primary mass flow rates and the critical back pressures.

Modélisation thermodynamique et détermination des paramètres de l'éjecteur pour des systèmes frigorifiques à éjection

Mots clés : Modélisation de l'éjecteur ; Système frigorifique à éjecteur ; Vérification expérimentale ; Détermination des paramètres ; Mode d'exploitation critique

1. Introduction

Various thermodynamic cycles have been proposed, studied and developed to utilise and recover low-grade heat for cooling purpose, such as absorption cycle, adsorption cycle, desiccant cycle and ejection cycle. Amongst all of these, the ejection technology has attracted exponentially increasing interests in recent years (Besagni et al., 2016; Chen et al., 2015; Elbel and Lawrence, 2016) as ejector refrigeration system has many merits

* *Corresponding author.* Sir Joseph Swan Centre for Energy Research, Newcastle University, Newcastle upon Tyne NE1 7RU, UK. Fax: +44 001912226920.
E-mail address: huashan.bao@newcastle.ac.uk (H. Bao).

http://dx.doi.org/10.1016/j.ijrefrig.2016.12.005

Nomenclature

A	area [m^2]
Ar_h	hypothetical throat area ratio [–]
Ar_n	nozzle throat area ratio [–]
C	sound speed [$m\ s^{-1}$]
h	enthalpy [$J\ kg^{-1}$]
Ma	mach number [–]
$\dot{m}$	mass flow rate [$kg\ s^{-1}$]
P	pressure [Pa]
Pr	pressure ratio [–]
s	entropy [$J\ (kg\ K)^{-1}$]
T	temperature [°C]
V	flow velocity [$m\ s^{-1}$]

Greeks

α	volume fraction [–]
η	efficiency [–]
ρ	density [$kg\ m^{-3}$]

Subscripts

1, 2, 3, 4	ejector section position
d	diffuser
is	isentropic
l	liquid
m	mixing
n	nozzle
p	primary
s	suction
tp	two phase
v	vapour

Superscripts

*	critical operation mode

such as structural simplicity, no moving parts, robust operation, desirable longevity, low cost and easy maintenance. However, its relatively low coefficient of performance is reckoned as the barrier of widespread application and commercialisation. Using industrial waste heat, solar energy or other types of renewable energy as the heat source for ejection refrigeration is recognised to fully realise its value and benefits. The ejector has also been integrated into other refrigeration systems to promote thermal efficiencies, such as vapour compression system and absorption system (Besagni et al., 2016; Chen et al., 2015; Elbel and Lawrence, 2016); moreover, the ejector has been applied to organic Rankine cycle (Yang et al., 2016) to achieve power and refrigeration cogeneration, and to Kalina cycle (Li et al., 2013) for performance improvement.

In an ejector, a high pressure primary fluid expands and accelerates to supersonic velocity by flowing through a converging–diverging nozzle. This creates a very low pressure at the downstream of the nozzle, therefore, a low pressure secondary fluid is sucked into the ejector and is entrained to a higher velocity. These two streams completely mix as the primary flow is retarded whilst the secondary flow is accelerated, and then they eventually become a single stream. Thereafter a normal shock wave is induced which is subjected to the moderate back pressure in the condenser of the refrigeration system, resulting in an abrupt pressure increase and sudden velocity drop down to subsonic area. The subsonic working fluid is subsequently compressed in the diffuser where the pressure is elevated to be higher than the initial pressure of the secondary flow while the velocity declines to nearly zero. Many studies have numerically modelled ejector and ejection process to conduct the device design and performance estimation and analysis (He et al., 2009). Basically, there are three different approaches of ejector modelling: thermodynamic modelling, one-dimensional and multi-dimensional modelling (Elbel and Lawrence, 2016; He et al., 2009). The latter two approaches require knowledge of computational fluid dynamic (CFD) and the usage of commercial CFD software. The powerful CFD method can obtain the flow details inside the ejector, it is however challenging to select and implement the turbulence model and mixing model within CFD mode. The thermodynamic method is the most commonly used for ejector numerical study due to its simplicity (Elbel and Lawrence, 2016; He et al., 2009).

In thermodynamic modelling method, the whole ejection process is divided into several sub-processes, they are in sequence the expansion in nozzle, the suction process, the mixing process, and the diffusion process. The thermodynamic states at beginning and end of each sub-process can be determined by using energy balance, momentum balance and mass balance equations. To solve the difficulty in establishing the momentum balance equation, Keenan et al. (Keenan and Neumann, 1942; Keenan et al., 1950) assumed the mixing process occurred either under constant pressure or within constant area. Up to now the majority of ejector thermodynamic models have been applying Keenan et al.'s hypotheses. Eames et al. (1995) proposed an upgraded model for a steam ejector in which isentropic efficiencies were introduced to each ejection subprocess so that the friction losses of the working fluid flow and the non-ideal mixing were taken into account. With the information of the pressure, temperature and mass flow rates of both primary flow and secondary flow, Eames et al. started the modelling with an assumed mixing pressure to carry out the iterative calculation that terminated when a maximum outlet pressure was obtained, in this instance, the critical condensation pressure was achieved for the ejector refrigeration system.

Postulated from experimental results, Munday and Bagster (1977) proposed an alternative theoretical ejection process that assumed the primary flow fanned out from the nozzle without mixing with the secondary flow in some downstream distance, and this part of primary flow was named as primary flow core in present paper. The diverging primary flow core resulted in a converging duct for the secondary flow so that the secondary flow was accelerated to sound speed (where the Mach number was 1) before the mixing process started. In this instance both the primary flow and secondary flow were choked, therefore the ejection reached its critical operation mode, in which the outlet pressure was the critical back pressure. Nevertheless, in this theory, the hypothetical throat area of the secondary flow remained unknown. Huang et al. (Huang and Chang, 1999; Huang et al., 1999) validated Munday and Bagster's hypothesis through experimental tests and numeri-

cal analysis on different sizes of ejectors using R141b as working fluid. The corresponding hypothetical throat area for the secondary flow was considered as the function of initial primary fluid pressure, initial secondary fluid pressure, critical back pressure and nozzle throat area. Zhu et al. (2007) developed a two dimensional (2D) 'shock circle model' based on Munday and Bagster's hypothesis, which employed non-uniform velocity distribution in the cross-sectional area at the hypothetical throat of secondary flow. It was found that the corresponding velocity reduced along the radial direction from the centre of primary flow core to the ejector wall, and the secondary flow reached sound speed at a certain radius. The authors claimed that this 2D model needed less numbers of pre-defined isentropic efficiencies and was more accurate than the model developed by Huang et al. (1999). Cardemil and Colle (2012) applied Munday and Bagster's hypothesis to a two-phase ejector. They introduced an isentropic parameter to estimate the cross sectional area of primary flow core before mixing, and determined this parameter based on some reported experimental results.

As aforementioned, a couple of trials have been made to determine the hypothetical throat area; however, they are not enough to draw a coincident conclusion of neither the determination method nor the value of this parameter; moreover, the general applicability of the model to different working fluids should be improved. The present paper aims at establishing a thermodynamic model for ejector with constant mixing area based on Munday and Bagster's hypothesis, and more importantly, determining empirical correlations of the hypothetical throat area based on several experimental tests using R141b, R134a and steam as working fluid. Different from the study reported by Huang et al. (Huang and Chang, 1999; Huang et al., 1999), present study aimed at the ejector performance evaluation rather than ideal ejector design under given operation condition; more importantly, real working fluid properties rather than ideal gas model were used, and the energy transfer between the primary flow core and the secondary flow was considered in present study to simulate the ejection process more realistically. The measured primary mass flow rates and critical back pressures (or saturated temperatures) in some reported experiments were used to verify the present model. The obtained empirical correlations will be useful for further ejector performance prediction.

2. Ejector model

The schematic diagram of an ejector with constant mixing area is shown in Fig. 1(a) and the corresponding pressure and velocity profiles based on Munday and Bagster's hypothesis are exemplified in Fig. 1(b). The primary flow enters the ejector at relatively high pressure (section p in Fig. 1(a)), and its pressure decreases while its velocity increases when flowing through the nozzle. The primary flow reaches the sound speed at the nozzle throat (section t), and even higher velocity at the nozzle exit (section 1) and further higher at the exit of primary flow core (section 2). The secondary flow (section s) is sucked into the ejector and is accelerated to sound speed at the hypothetical throat (section 2) formed by the boundary of the primary flow core and the ejector wall, as shown in Fig. 1(a), in the meantime its pressure reduces to the value as the same as that of the primary fluid at section 2. The mixing takes place between sections 2 and 3, where the pressure of the mixed stream increases due to the constant mixing area. The normal shock occurs at section 'sh' where the pressure increases and the velocity drops to subsonic level. Finally, the pressure of the working fluid is promoted and the velocity drops after flowing through the diffuser (from section 4 to d).

The thermodynamic model is established based on mass balance, momentum balance and energy balance equations. During the ejection process, the working fluid may become liquid-vapour two-phase if the fluid is so-called 'wet fluid'. The present model treats the working fluid as homogeneous despite of single-phase or two-phase, and this indicates that the possible relative motion between two phases is eliminated. Homogeneous equilibrium is assumed here to simplify the model, thus the heat transfer between phases occurs instantaneously and the thermodynamic equilibrium is ensured. Hence, the flows inside the ejector can be treated as steady and one-dimensional. Other assumptions to simplify the model without losing the generality are given as follows.

- The flow is adiabatic.
- The kinetic energies at the inlets of both primary flow and secondary flow are negligible.
- Flow friction leads to non-isentropic expansion/diffusion process in ejector, which is reflected by isentropic efficiencies.
- The inefficient momentum transfer in the non-ideal mixing is represented by a mixing loss factor.

All the thermodynamic property data of different working fluids are provided by NIST Refprop 9.1 (Lemmon et al., 2013).

2.1. *Nozzle throat and outlet*

According to the foregoing assumption, the expansion process is non-isentropic and an isentropic efficiency, η_n is given for the working fluid in both the converging and diverging sections as expressed by Eqs. (1) and (2).

$$\eta_n = \frac{h_p - h_t}{h_p - h_{t,is}} \tag{1}$$

$$\eta_n = \frac{h_t - h_{p1}}{h_t - h_{p1,is}} \tag{2}$$

where the subscripts p, t and p1 denote primary flow at nozzle inlet, throat and outlet, respectively; $h_{t,is}$ and $h_{p1,is}$ are the enthalpies if the expansion processes are isentropic, which can be calculated based on the present pressure and the previous entropy, as expressed in Eqs. (3) and (4).

$$h_{t,is} = h(P_t, s_p) \tag{3}$$

$$h_{p1,is} = h(P_{p1}, s_t) \tag{4}$$

Applying the energy conservation to the nozzle, Eqs. (5) and (6) can be obtained.

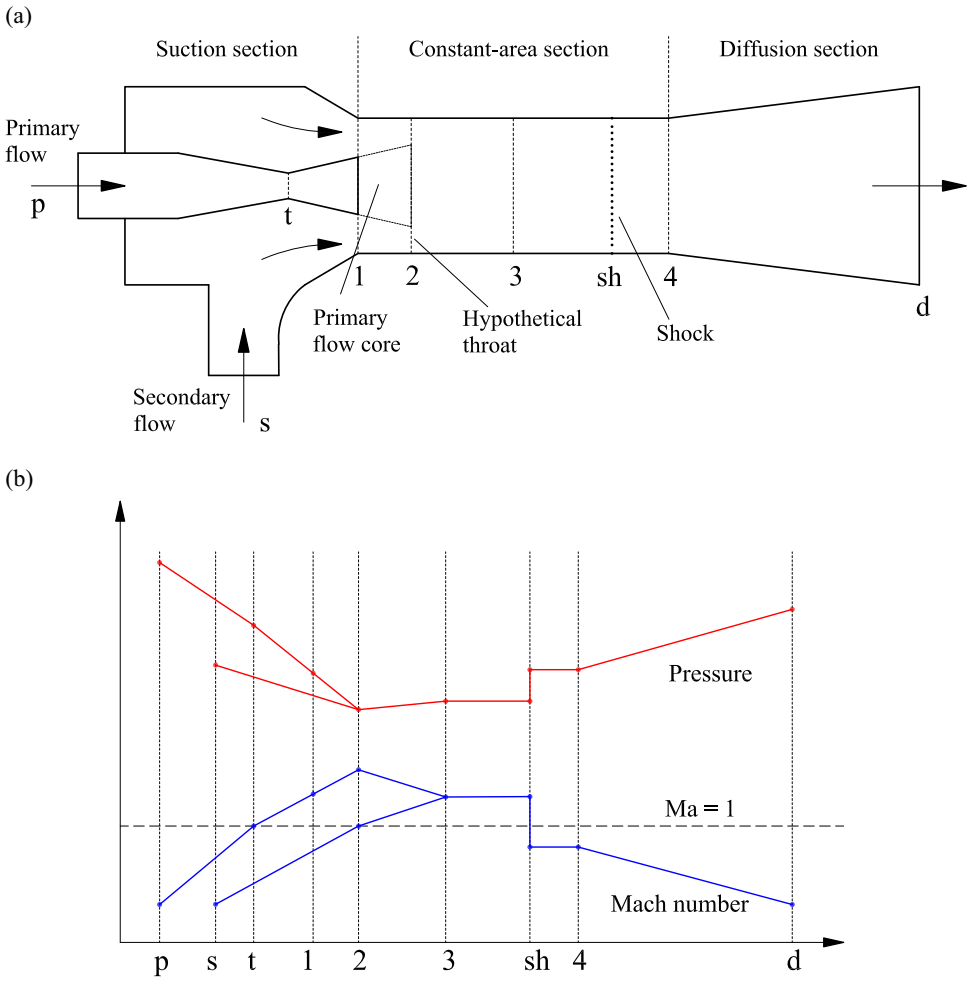

Fig. 1 – Schematic diagram of ejector and the corresponding pressure and velocity profiles based on Munday and Bagster's hypothesis.

$$h_p = h_t + \frac{V_t^2}{2} \tag{5}$$

$$h_t + \frac{V_t^2}{2} = h_{p1} + \frac{V_{p1}^2}{2} \tag{6}$$

where V_t and V_{p1} are the primary flow velocities at the throat and the outlet of the nozzle, respectively. V_t equals to the sound speed which can be calculated based on the thermodynamic states of the working fluid by Eq. (7).

$$V_t = C(P_t, h_t) \tag{7}$$

Thereafter the mass flow rate of the primary flow can be derived as Eq. (8).

$$\dot{m}_p = \dot{m}_t = \rho_t A_t V_t \tag{8}$$

where A_t is the cross sectional area of the throat; the working fluid density at throat, ρ_t, can be calculated based on the corresponding pressure and enthalpy as Eq. (9).

$$\rho_t = \rho(P_t, h_t) \tag{9}$$

The velocity of the primary flow at the outlet of the nozzle, V_{p1}, is governed by the mass balance equation and can be calculated as Eq. (10).

$$V_{p1} = \frac{\dot{m}_p}{A_{p1}\rho_{p1}} \tag{10}$$

where A_{p1} is the cross sectional area of the nozzle outlet; the working fluid density, ρ_{p1}, is the function of pressure and enthalpy as expressed in Eq. (11).

$$\rho_{p1} = \rho(P_{p1}, h_{p1}) \tag{11}$$

2.2. *Suction and primary flow core*

According to Munday and Bagster's hypothesis, the secondary flow reaches the sound speed at the hypothetical throat, which can be formulated as Eq. (12).

$$V_{s2} = C(P_{s2}, h_{s2}) \tag{12}$$

Similar to the expansion process in nozzle, the governing equations for suction process are in the form of Eqs. (13) to (16).

$$\eta_s = \frac{h_s - h_{s2}}{h_s - h_{s2,is}} \tag{13}$$

$$h_{s2,is} = h(P_{s2}, s_s) \tag{14}$$

$$\dot{m}_s = V_{s2} A_{s2} \rho_{s2} \tag{15}$$

$$\rho_{s2} = \rho(P_{s2}, h_{s2}) \tag{16}$$

Although the mixing of the primary and secondary flows is expected to occur after the choke of the secondary flow, these two flow streams have energy transfer between each other within the sections 1 and 2 to implement the entrainment. The energy balance must be complied with as Eq. (17).

$$\dot{m}_p\left(h_{p1} + \frac{V_{p1}^2}{2}\right) + \dot{m}_s h_s = \dot{m}_p\left(h_{p2} + \frac{V_{p2}^2}{2}\right) + \dot{m}_s\left(h_{s2} + \frac{V_{s2}^2}{2}\right) \tag{17}$$

The primary flow core can be considered as the extension of the diverging expansion in the nozzle, hence the following governing equations [Eqs. (18) to (20)] are used in the present model.

$$\eta_n = \frac{h_{p1} - h_{p2}}{h_{p1} - h_{p2,is}} \tag{18}$$

$$h_{p2,is} = h(P_{p2}, s_{p1}) \tag{19}$$

$$\dot{m}_p = A_{p2} \rho_{p2} V_{p2} \tag{20}$$

$$\rho_{p2} = \rho(P_{p2}, h_{p2}) \tag{21}$$

where P_{p2} and P_{s2} have the same value, i.e. $P_{p2} = P_{s2} = P_2$; the cross sectional areas at section 2 satisfy the rule expressed in Eq. (22).

$$A_{p2} + A_{s2} = A_2 \tag{22}$$

2.3. Mixing process

The mixing process (sections 2–3) can be described by using the mass balance equation [Eq. (23)], energy balance equation [Eq. (24)], momentum balance equation [Eq. (25)], and thermodynamic state equation [Eq. (26)].

$$\rho_3 V_3 A_3 = \dot{m}_p + \dot{m}_s = \dot{m}_3 \tag{23}$$

$$\dot{m}_p\left(h_{p2} + \frac{V_{p2}^2}{2}\right) + \dot{m}_s\left(h_{s2} + \frac{V_{s2}^2}{2}\right) = \dot{m}_3\left(h_3 + \frac{V_3^2}{2}\right) \tag{24}$$

$$\eta_m\left(\dot{m}_p V_{p2} + \dot{m}_s V_{s2}\right) + P_{p2} A_{p2} + P_{s2} A_{s2} = \dot{m}_3 V_3 + P_3 A_3 \tag{25}$$

$$\rho_3 = \rho(P_3, h_3) \tag{26}$$

where η_m is the mixing loss factor, which accounts for the inefficient momentum transfer between primary and secondary flows due to the frictions between flows and between fluid and ejector wall.

2.4. Shock wave

A normal shock takes place in the constant-area section which induces a sharp pressure increase and velocity decrease. The Mach number of the working fluid is larger than 1 before this shock, whereas smaller than 1 after the shock. This process is irreversible and cannot be treated as isentropic. The process can be described by using the mass balance equation [Eq. (27)], energy balance equation [Eq. (28)] and momentum balance equation [Eq. (29)] and thermodynamic state equation [Eq. (30)].

$$\rho_3 V_3 = \rho_4 V_4 = \dot{m}_3 / A_3 \tag{27}$$

$$h_3 + \frac{V_3^2}{2} = h_4 + \frac{V_4^2}{2} \tag{28}$$

$$P_3 A_3 + \dot{m}_3 V_3 = P_4 A_3 + \dot{m}_3 V_4 \tag{29}$$

$$\rho_4 = \rho(P_4, h_4) \tag{30}$$

2.5. Diffusion process

The working fluid has been decelerated to subsonic after shock, so that a diffusion process occurs in the diverging diffuser, during which the pressure ascends and the velocity descends. The energy balance of this diffusion is established as Eq. (31).

$$h_d + \frac{V_d^2}{2} = h_4 + \frac{V_4^2}{2} \tag{31}$$

The working fluid can be decelerated to stagnant, i.e. $V_d = 0$, to recover the pressure as much as possible. This compression process has the isentropic efficiency η_d that is formulated as Eq. (32).

$$\eta_d = \frac{h_{d,is} - h_4}{h_d - h_4} \tag{32}$$

The outlet pressure, P_d, can be derived using the thermodynamic state equation [Eq. (33)] with the isentropic enthalpy $h_{d,is}$ and the entropy s_4 at the inlet of diffuser.

$$P_d = P(h_{d,is}, s_4) \tag{33}$$

Because the designed working conditions cannot be achieved in most practical operations of the ejector, the outlet velocity, V_d, cannot be treated as 0 and the mass balance equation [Eq. (34)] must be satisfied.

$$\dot{m}_d = \dot{m}_3 = \rho_d V_d A_d \tag{34}$$

where A_d is the diffuser outlet area and ρ_d is the working fluid density which can be determined by Eq. (35).

$$\rho_d = \rho(P_d, h_d) \tag{35}$$

2.6. Sound speed

For single phase working fluid, the local sound speed can be readily obtained by using NIST Refprop 9.1. Two-phase flow may occur in ejector when the used working fluid is not dry, and it is sophisticated to calculate the accurate sound speed of liquid-vapour two-phase flow. Several correlations have been proposed to estimate the sound speed of liquid-vapour two-phase flow based on the densities, volume fractions and sound speeds of liquid phase and vapour phase. One successful correlation, Eq. (36), proposed by Nguyen et al. (1981) was used in the present model. This correlation considers the interface on one phase acting as the elastic wall of the other phase, and it has been verified by both cavitation flow (low volume fraction of vapour phase) and condensing flow (high volume fraction of vapour phase).

$$C_{tp}^2 = \frac{1}{(1-\alpha)\sqrt{\frac{1-\alpha}{C_l^2}+\frac{\alpha\rho_l}{\rho_v C_v^2}}+\alpha\sqrt{\frac{\alpha}{C_v^2}+\frac{(1-\alpha)\rho_v}{\rho_l C_l^2}}} \quad (36)$$

3. Simulation process

The mathematical model described in Section 2 was programmed using Matlab. It should be mentioned that the present simulation required the input of the experimental critical entrainment ratio (the primary mass flow rate to the secondary mass flow rate at the critical operation mode) to obtain the hypothetical area for the secondary flow. The simulation was conducted in steps as shown in Fig. 2 and described in detail as follows.

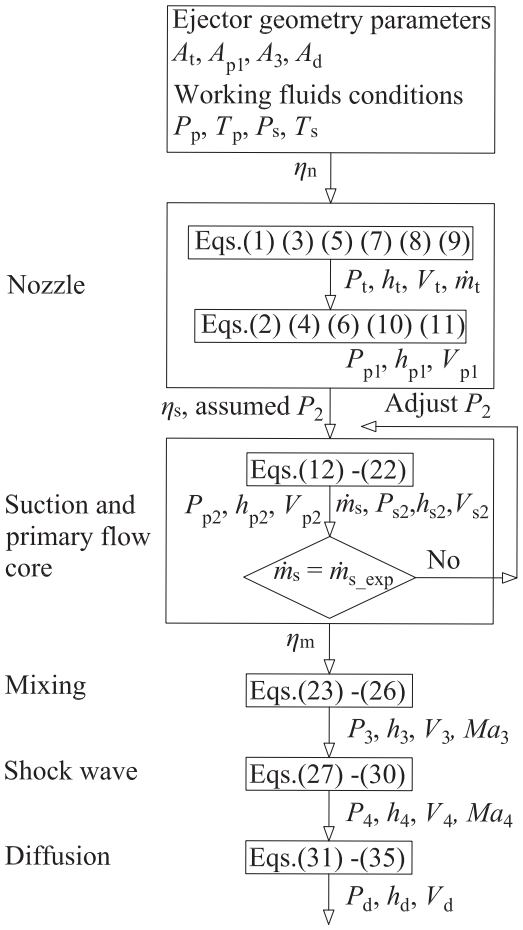

Fig. 2 – Flowchart of the present simulation process.

(1) Input geometric parameters of the ejector, including nozzle throat area, nozzle outlet area, mixing area and diffuser outlet area; input inlet pressures and temperatures of primary flow and secondary flow.

(2) With an assumed value of the pressure P_t at the nozzle throat, the isentropic enthalpy $h_{t,is}$ is obtained through Eq. (3); the real enthalpy h_t is calculated using Eq. (1) with a pre-defined nozzle isentropic efficiency η_n; the flow velocity V_t is determined by the energy balance equation [Eq. (5)]; the local sound speed of working fluid is calculated based on P_t and h_t via Eq. (7). The contrast between V_t and the local sound speed triggers an iteration process, i.e. the value of P_t is re-assumed and the foregoing calculation is repeated until the obtained V_t equals to the local sound speed. The primary mass flow rate $\dot{m}_p$ can be calculated by Eq. (8) with the density determined by Eq. (9) and the given throat area A_t.

(3) With an assumed value of pressure P_{p1} at the nozzle outlet, the isentropic enthalpy $h_{p1,is}$ is calculated using Eq. (4); the real enthalpy h_{p1} is acquired by Eq. (2) with the isentropic efficiency η_n pre-defined in step 2; the flow velocity V_{p1} is determined by the energy balance equation, Eq. (6); the density at nozzle exit ρ_{p1} is calculated based on P_{p1} and h_{p1} via Eq. (11); meanwhile, the V_{p1} can also be calculated by the mass balance equation [Eq. (10)] with the obtained mass flow rate $\dot{m}_p$ in step 2; then the iteration starts as the P_{p1} is adjusted to repeat the foregoing calculation until the sufficiently small discrepancy between the two velocities (V_{p1}) obtained by two different routes is achieved.

(4) A value of P_2 at the section 2 is assumed to start this step of calculation; the isentropic enthalpy $h_{s2,is}$ is calculated through Eq. (14); the real enthalpy h_{s2} is calculated by Eq. (13) with a pre-defined suction isentropic efficiency η_s; the density of secondary fluid at section 2, ρ_{s2} is calculated based on P_{s2} and h_{s2} by Eq. (16); similarly, the enthalpy and density of primary flow at section 2, h_{p2} and ρ_{p2}, can be obtained based on Eqs. (18), (19) and (21); the flow velocity of secondary flow, V_{s2}, which is at the sound speed, can be determined by Eq. (12); the experimental entrainment ratio ($\dot{m}_s/\dot{m}_p$) is used here to calculate the mass flow rate of secondary flow, $\dot{m}_s$; then the hypothetical throat area, A_{s2}, is calculated by using Eq. (15); since the mixing area is already known, the primary flow core end area A_{p2} can be easily obtained by Eq. (22); thereafter the flow velocity V_{p2} is calculated by Eq. (20). An iterative calculation is required to achieve the energy balance described in Eq. (17), i.e. to start over this step of calculation with a new reasonable P_2 to repeat the above procedure until the Eq. (17) is satisfied.

(5) A value of pressure P_3 at the section 3 is initially assumed; the flow velocity V_3 after mixing is then calculated by

the momentum balance equation [Eq. (25)] with a predefined mixing loss factor, η_m; the enthalpy h_3 is obtained by solving the energy balance equation [Eq. (24)]; then the fluid density ρ_3 can be obtained based on the state equation, Eq. (26); an iteration is conducted by adjusting P_3 to satisfy the mass balance equation, Eq. (23).

(6) The equations of shock wave, Eqs. (27) to (30), can be solved following the same method given in step 5.

(7) If the designed working conditions of the ejector can be satisfied, the exit velocity V_d of the diffuser can be considered at 0, therefore, the enthalpy h_d can be calculated by Eq. (31) and the pressure P_d at the ejector outlet is obtained through Eqs. (32) and (33).

(8) If the designed working conditions cannot be ensured, the diffuser outlet area should be known, and an outlet velocity V_d should be initially assumed to start iterative calculation to achieve mass balance: with an assumed outlet velocity V_d, the corresponding outlet pressure P_d and enthalpy h_d can be obtained as described in step 7; the density ρ_d is then calculated by Eq. (35); the mass balance equation [Eq. (34)] is checked before a new velocity is assumed accordingly if necessary to start over the calculation.

In the end, the obtained empirical hypothetical throat area of the secondary flow was analysed and correlated with relevant variables, which would be critically significant for further ejector performance estimation.

4. Experimental verification and parameter determination

The thermodynamic modelling of the ejector was criticised on the artificial selection of the used isentropic efficiencies and the lack of justification (Elbel and Lawrence, 2016). The present study aimed at promoting this method by introducing the experiment results to determine the key parameter, the hypothetical throat area, for further modelling, so that the uncertainty of the modelling did not highly rely on those isentropic efficiencies any more but more depended on the hypothetical throat area which was determined by experimental results. To determine this area, the usage of experimental obtained $\dot{m}_s/\dot{m}_p$ at critical operation mode was essential. However, the present experiment-involved modelling can still be verified. First, the calculated mass flow rate of primary flow was only the function of its initial pressure, temperature and the nozzle throat area, then this calculation can be validated by using the available experimental measured mass flow rate of primary flow; secondly, the introduced experimental $\dot{m}_s/\dot{m}_p$ only had a little influence on the thermodynamic state at the outlet of ejector, therefore the accuracy of the present modelling can be verified by the experimental thermodynamic state of the working fluid at the outlet of ejector.

Referring to the efficiencies proposed by different researchers (summarised by Liu and Groll, 2013), $\eta_n = 0.95$, $\eta_s = 0.85$, $\eta_m = 0.95$ and $\eta_d = 0.85$ were initially selected as the basic values as these values have been used in many works. Nevertheless, if the measured primary mass flow rate was available, the exact nozzle efficiency η_n would be experimentally determined. Moreover, the mixing loss factor η_m should be adjusted if non-negligible amount of liquid appeared during ejection, which will be discussed in details later.

4.1. Nozzle and sound speed

Since the primary flow is choked at the nozzle throat, the primary flow rate is a constant value if the inlet pressure and temperature and throat area are pre-defined. The accuracy of this calculated mass flow rate highly depends on the accuracy of the calculated sound speed.

Three experimentally measured values of primary mass flow rate (Eames et al., 1999; Shestopalov et al., 2015; Thongtip and Aphornratana, 2015) and one two-dimensional (2D) CFD simulation result (Varga et al., 2009) were compared with the calculated results by the present model. Fig. 3(a) shows perfect agreements between the calculated values and the measured values of primary mass flow rates when the working fluids are R141b (Thongtip and Aphornratana, 2015) and R245fa (Shestopalov et al., 2015). When the nozzle isentropic efficiencies of 0.93 and 1.0 were used for R141b and R245fa, respectively, the discrepancies are within ±5% regardless of different nozzle throat areas. It should be noted that these two working fluids are dry vapours through along the nozzle. It is in liquid-vapour two-phase during the ejection process if the working fluid is steam because water is a wet fluid, consequently the sound speed should be calculated by Eq. (36) rather than by NIST 9.1 that only provides the data of single phase. Fig. 3(b) exhibits the contrast between the calculated results and the experimental results (Eames et al., 1999) and the 2D CFD simulation result (Varga et al., 2009) using steam as the working fluid under the conditions of different throat areas and different inlet pressures and temperatures. The vapour quality at the throat was in the range of 0.96–0.97 according to present calculation. It is noticeable that the present calculation slightly underestimates the primary mass flow rate even the isentropic efficiencies were defined as 1.0 in both comparisons, however, with acceptable discrepancies in the range of ±5%.

4.2. Critical back condition

The critical operation mode of the ejector is defined as the condition when the primary and secondary flows are both choked; in this instance, the corresponding back pressure and the entrainment ratio are the critical back pressure and critical entrainment ratio, respectively. If the back pressure is higher than the critical value, only primary flow is choked and the entrainment ratio increases with the decreasing back pressure; if the back pressure is lower than the critical value, the decrease of back pressure cannot lead to any increment of entrainment ratio due to the double-choked. Since the secondary flow was assumed to be choked at the hypothetical throat, the current calculation was only for the critical operation mode.

As aforementioned, the critical entrainment ratio and the critical back pressure are two essential parameters for performance evaluation. As the hypothetical throat for secondary flow was unknown, the experimentally obtained critical entrainment ratio was introduced into the calculation of the present model, and the accuracy of this numerical simulation can be

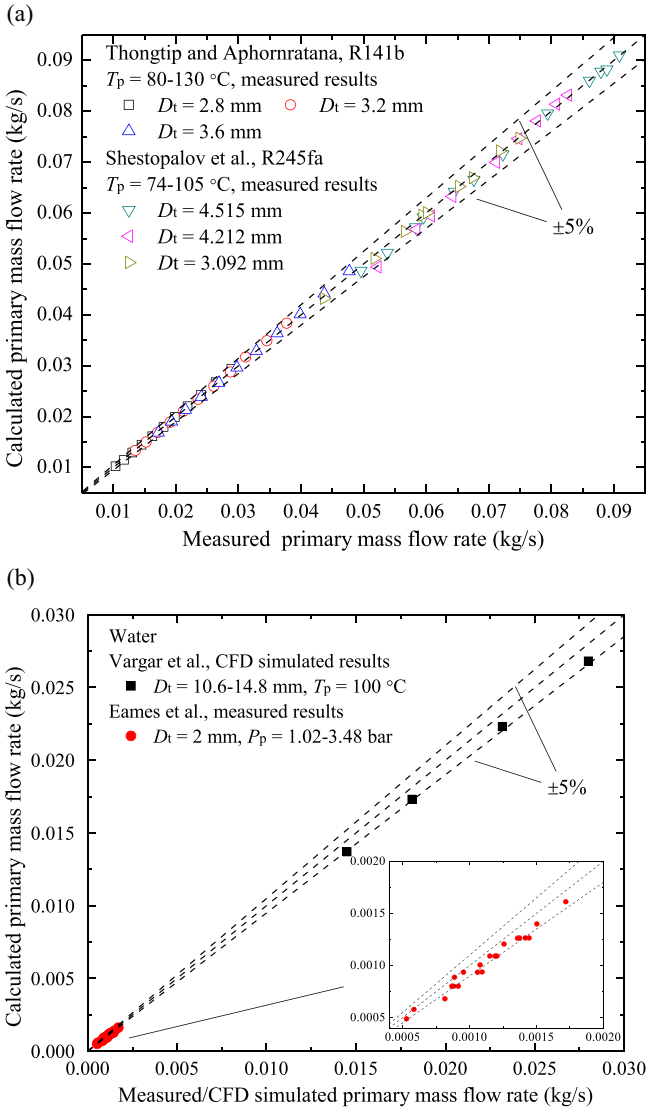

Fig. 3 – Comparison between measured/CFD simulated primary mass flow rates and the calculated values, (a) η_n = 0.93 for R141b reported by Thongtip and Aphornratana (2015), η_n = 1.0 for R245fa reported by Shestopalov et al. (2015); (b) η_n = 1.0 for steam reported by Eames et al. (1999) and Varga et al. (2009).

ensured and reflected by the comparison between the calculated values and the measured values of the critical back pressure (or saturation temperature). Tables 1 to 6 summarise the comparison between the calculated results in this work and six sets of experimental results reported in Chen and Sun (1997), Eames et al. (1999), Garcia del Valle et al. (2014), Huang et al. (1999), Thongtip and Aphornratana (2015), and Yan and Cai (2012), among which two cases had R141b as working fluid, two cases used R134a and the other two cases used steam as working fluid.

As presented in Table 1, Huang et al. (1999) tested R141b using ejectors with different nozzle throat areas, nozzle exit areas and mixing areas. The calculated critical back saturated temperatures based on the present model agree with the measured values perfectly with a discrepancy in the range of –4.79% to 3.11%, when the employed isentropic efficiencies were η_n = 0.95, η_s = 0.85, η_m = 0.95 and η_d = 0.85. Using the same working fluid, Thongtip and Aphornratana (2015) tested a slightly larger ejector through two different analytical methods: one method was to determine the critical back pressure (condensing pressure) with a fixed primary flow pressure (generating pressure) and a fixed secondary flow pressure (evaporating pressure), and the other one was to determine the critical secondary flow pressure at a fixed primary flow pressure and a fixed back pressure. As shown in Table 2, the calculated critical back pressures in this work agreed well with the measured values by Thongtip and Aphornratana's first experimental method, with a discrepancy in the range of –4.78% to 5.19%, when the employed isentropic efficiencies were η_n = 0.93 (determined by the given measured primary flow rate), η_s = 0.85, η_m = 0.95 and η_d = 0.85; whereas, larger errors of the critical evaporator pressure were generated when compared with the measured value by the second experimental method.

As revealed in Tables 3 and 4, good agreements can be achieved between the predicted critical back conditions based on present model and the measured values by Garcia del Valle et al. (2014) and Yan and Cai (2012) when using R134a as working fluid, and the discrepancies were in the range of –1.26% to 6.08% and –7.85% to 9.00% respectively, when η_n = 0.95, η_s = 0.85, η_m = 0.95 and η_d = 0.85 were used. These two sets of experiments used similar size ejector and close working fluid pressures. Since R134a is a wet fluid, Valle et al.'s experiments used 10 °C superheating for both primary fluid and secondary fluid, as a result no liquid occurs during the ejection according to the present calculation; whereas, Yan and Cai's experiment employed saturated vapour for ejection, resulting in two-phase flow inside the ejector, that implies that two-phase sound speed correlation should be used in the calculation. However, the calculation accuracy based on the two-phase sound speed correlation is not as good as that for single-phase vapour by using NIST 9.1. Therefore, relatively larger discrepancies contrasted with the reported values by Yan and Cai (2012) were noticed as given in the table.

Using saturated steam as working fluid can lead to the appearance of liquid in both primary and secondary fluid flows because steam is a wet fluid. For the experiments reported by Eames et al. (1999) and Chen and Sun (1997), the calculated vapour quality of the primary flow based on the present model could be lower than 0.8 at the ejector section 2, which suggests a high mixing loss between the primary and secondary flows. Under this circumstance, the mixing loss factor η_m at 0.67 and 0.72 gave the smallest calculation error for these two study cases respectively, when using η_n = 1, η_s = 0.85 and η_d = 0.85 (η_n was determined as 1 by the measured primary flow rate as discussed in Section 4.1). The calculation errors of the back conditions for these two study cases are all around ±5% as presented in Tables 5 and 6.

4.3. *Hypothetical throat area*

For ejector design purpose, Huang et al. (Huang and Chang, 1999; Huang et al., 1999) have developed an empirical correlation of the hypothetical throat area as the function of P_p, P_s and P_d^* based on ideal gas model. However, their method was not suitable to estimate the performance of ejector when the ejector

Table 1 – Verification of present modelling and the obtained hypothetical throat area ratio, with R141b as the working fluid by Huang et al. (1999), $\eta_n = 0.95$, $\eta_s = 0.85$, $\eta_m = 0.95$, $\eta_d = 0.85$.

D_t (mm)	D_{p1} (mm)	D_3 (mm)	P_p (bar)	P_s (bar)	ω^* (–)	T_d^*, sat. (°C)			Ar_h (–)
						Exp.	Sim.	Error (%)	
2.82	5.10	9.20	6.04	0.40	0.438	31.30	31.49	0.60	0.517
2.82	5.10	8.84	6.04	0.40	0.394	33.00	33.05	0.16	0.489
2.64	4.50	8.10	6.04	0.40	0.346	33.60	33.71	0.33	0.458
2.82	5.10	8.54	6.04	0.40	0.351	34.20	34.39	0.55	0.459
2.64	4.50	7.60	6.04	0.40	0.281	36.30	36.33	0.08	0.406
2.82	5.10	8.10	6.04	0.40	0.290	37.10	36.51	–1.59	0.412
2.82	5.10	7.60	6.04	0.40	0.227	38.80	39.20	1.03	0.353
2.64	4.50	7.34	6.04	0.40	0.255	38.60	37.86	–1.92	0.381
2.82	5.10	7.34	6.04	0.40	0.204	41.00	40.79	–0.52	0.327
2.64	4.50	6.70	6.04	0.40	0.186	42.10	41.95	–0.36	0.306
2.64	4.50	8.10	5.38	0.40	0.445	31.50	31.33	–0.54	0.514
2.64	4.50	7.60	5.38	0.40	0.349	33.80	33.61	–0.55	0.454
2.64	4.50	7.34	5.38	0.40	0.304	36.70	34.94	–4.79	0.420
2.64	4.50	6.98	5.38	0.40	0.272	37.50	37.16	–0.92	0.389
2.64	4.50	6.70	5.38	0.40	0.225	38.90	38.82	–0.22	0.344
2.64	4.50	8.10	4.65	0.40	0.539	28.00	28.18	0.64	0.557
2.64	4.50	7.60	4.65	0.40	0.424	30.50	30.23	–0.88	0.498
2.64	4.50	7.34	4.65	0.40	0.388	32.30	31.58	–2.22	0.474
2.64	4.50	6.98	4.65	0.40	0.312	33.60	33.35	–0.74	0.420
2.64	4.50	6.70	4.65	0.40	0.288	35.50	35.13	–1.04	0.398
2.64	4.50	8.10	4.00	0.40	0.623	24.40	24.95	2.27	0.589
2.64	4.50	7.60	4.00	0.40	0.489	26.90	26.78	–0.46	0.531
2.64	4.50	7.34	4.00	0.40	0.439	29.10	27.96	–3.92	0.503
2.64	4.50	6.98	4.00	0.40	0.392	29.50	29.90	1.34	0.472
2.64	4.50	6.70	4.00	0.40	0.326	32.50	31.26	–3.82	0.426
2.82	5.10	8.84	6.04	0.47	0.499	33.10	34.13	3.11	0.541
2.82	5.10	8.54	6.04	0.47	0.405	34.20	35.03	2.43	0.492
2.64	4.50	8.10	6.04	0.47	0.454	34.50	34.81	0.90	0.518
2.64	4.50	7.34	6.04	0.47	0.350	38.70	38.82	0.30	0.449
2.82	5.10	7.60	6.04	0.47	0.304	39.30	39.99	1.75	0.415
2.64	4.50	6.70	6.04	0.47	0.235	42.50	42.48	–0.05	0.353
2.64	4.50	8.10	5.38	0.47	0.542	32.00	32.36	1.11	0.558
2.64	4.50	7.34	5.38	0.47	0.403	36.00	35.95	–0.13	0.481
2.64	4.50	6.70	5.38	0.47	0.295	39.50	39.55	0.12	0.402
2.64	4.50	8.10	4.65	0.47	0.635	28.90	29.21	1.06	0.593
2.64	4.50	7.34	4.65	0.47	0.479	32.40	32.55	0.46	0.520
2.64	4.50	6.70	4.65	0.47	0.340	36.00	35.74	–0.72	0.435
2.64	4.50	8.10	4.00	0.47	0.741	25.70	26.16	1.79	0.626
2.64	4.50	7.34	4.00	0.47	0.613	29.20	29.60	1.36	0.573

geometry, primary and secondary fluid pressures and temperatures were initially known. In this work, for ejector performance estimation purpose, the ratio value of the hypothetical throat area to the constant mixing area, $Ar_h = A_{s2}/A_3$, was pursued, afterwards the critical entrainment ratio ω^* and back pressure P_d^* (or saturated temperature T_d^*) can be determined by the present model. Tables 1 to 6 present the obtained Ar_h. Two non-dimensional parameters, $Ar_n = A_t/A_3$ and $Pr = P_p/$

Table 2 – Verification of present modelling and the obtained hypothetical throat area ratio, with R141b as the working fluid by Thongtip and Aphornratana (2015), $\eta_n = 0.93$, $\eta_s = 0.85$, $\eta_m = 0.95$, $\eta_d = 0.85$.

D_t (mm)	D_{p1} (mm)	D_3 (mm)	D_d (mm)	T_p (°C)	T_s (°C)	ω^* (–)	P_d^* (bar)			Ar_h (–)
							Exp.	Sim.	Error (%)	
3.20	7.06	9.50	24.00	100.0	–4.0	0.020	0.92	0.968	5.19	0.050
3.20	7.06	9.50	24.00	100.0	–2.0	0.040	0.96	0.973	1.31	0.096
3.20	7.06	9.50	24.00	100.0	0.0	0.062	1.00	0.978	–2.21	0.138
3.20	7.06	9.50	24.00	100.0	2.0	0.110	1.04	0.990	–4.78	0.217
3.20	7.06	9.50	24.00	120.0	2.0	0.062	1.00	1.495	49.49	0.136
3.20	7.06	9.50	24.00	110.0	–4.0	0.012	1.00	1.203	20.27	0.031
3.20	7.06	9.50	24.00	90.0	4.0	0.224	1.00	0.814	–18.58	0.354
2.80	6.04	9.50	24.00	110.0	2.0	0.149	1.00	0.987	–1.32	0.280
3.20	7.06	9.50	24.00	110.0	0.0	0.062	1.00	1.216	21.57	0.137

Table 3 – Verification of present modelling and the obtained hypothetical throat area ratio, with R134a as the working fluid by Garcia del Valle et al. (2014), $\eta_n = 0.95$, $\eta_s = 0.85$, $\eta_m = 0.95$, $\eta_d = 0.85$.

D_t (mm)	D_{p1} (mm)	D_3 (mm)	D_d (mm)	T_p[a] (°C)	T_s[a] (°C)	ω^* (–)	T_d^*, sat. (°C)			Ar_h (–)
							Exp.	Sim.	Error (%)	
2.0	3.0	4.8	10.0	89.37	17.0	0.422	28.95	28.59	–1.26	0.470
2.0	3.0	4.8	10.0	89.37	20.0	0.494	29.41	29.53	0.42	0.504
2.0	3.0	4.8	10.0	94.39	17.0	0.342	31.68	31.35	–1.05	0.424
2.0	3.0	4.8	10.0	94.39	20.0	0.398	32.48	32.12	–1.10	0.457
2.0	3.0	4.8	10.0	99.15	15.0	0.273	32.02	33.97	6.08	0.374
2.0	3.0	4.8	10.0	99.15	17.0	0.297	34.11	34.33	0.64	0.392
2.0	3.0	4.8	10.0	99.15	20.0	0.339	35.41	34.94	–1.32	0.420

[a] 10 °C superheating was used.

P_s, were proposed in this work to develop a correlation of Ar_h. The former one reflects the ejector geometry while the latter one accounts for the fluid conditions. Fig. 4 shows the relationship between the obtained values Ar_h and $PrAr_n$ for all working fluids experimented in Chen and Sun (1997), Eames et al. (1999), Garcia del Valle et al. (2014), Huang et al. (1999), Thongtip and Aphornratana (2015), and Yan and Cai (2012).

Except that the present model had large error when predicting the critical evaporating pressure for the experiments reported by Thongtip and Aphornratana (2015) as mentioned

Table 4 – Verification of present modelling and the obtained hypothetical throat area ratio, with R134a as the working fluid by Yan and Cai (2012), $\eta_n = 0.95$, $\eta_s = 0.85$, $\eta_m = 0.95$, $\eta_d = 0.85$.

D_t (mm)	D_{p1} (mm)	D_3 (mm)	P_p (bar)	P_s (bar)	ω^* (–)	P_d^* (bar)			Ar_h (–)
						Exp.	Sim.	Error (%)	
2.5	4.1	4.8	20.50	4.43	0.276	8.40	8.13	–3.27	0.351
2.5	4.1	4.8	20.50	4.14	0.220	8.40	7.96	–5.24	0.307
2.5	4.1	4.8	20.50	3.88	0.140	8.40	7.74	–7.85	0.226
2.5	4.1	5.1	23.50	4.43	0.302	8.10	8.51	5.11	0.376
2.5	4.1	5.1	23.50	4.14	0.254	8.10	8.36	3.22	0.341
2.5	4.1	5.1	23.50	3.88	0.172	8.10	8.13	0.34	0.267
2.2	3.8	4.8	25.00	4.43	0.403	7.70	8.39	9.00	0.445
2.2	3.8	4.8	25.00	4.14	0.318	7.70	8.15	5.84	0.396
2.2	3.8	4.8	25.00	3.88	0.215	7.70	7.86	2.14	0.316

Table 5 – Verification of present modelling and the obtained hypothetical throat area ratio, with water as the working fluid by Eames et al. (1999), $\eta_n = 1.0$, $\eta_s = 0.85$, $\eta_m = 0.67$, $\eta_d = 0.85$.

D_t (mm)	D_{p1} (mm)	D_3 (mm)	D_d (mm)	T_p (°C)	T_s (°C)	ω^* (–)	T_d^*, sat. (°C)			Ar_h (–)
							Exp.	Sim.	Error (%)	
2.0	8.0	18.0	77.0	120.0	5.0	0.32	24.00	25.38	5.75	0.546
2.0	8.0	18.0	77.0	130.0	5.0	0.27	31.15	30.31	–4.66	0.509

Table 6 – Verification of present modelling and the obtained hypothetical throat area ratio, with water as the working fluid by Chen and Sun (1997), $\eta_n = 1.0$, $\eta_s = 0.85$, $\eta_m = 0.72$, $\eta_d = 0.85$.

D_t (mm)	D_{p1} (mm)	D_3 (mm)	P_p (bar)	P_s (bar)	ω^* (–)	P_d^* (bar)			Ar_h (–)
						Exp.	Sim.	Error (%)	
2.0	9.3	17.8	1.53	0.0131	0.492	0.0294	0.0300	2.030	0.638
2.0	9.3	17.8	1.53	0.0193	0.796	0.0315	0.0330	4.526	0.731
2.0	9.3	17.8	1.53	0.0235	0.995	0.0345	0.0349	1.237	0.768
2.0	9.3	17.8	1.98	0.0131	0.394	0.0393	0.0374	–4.831	0.591
2.0	9.3	17.8	1.98	0.0193	0.644	0.0410	0.0405	–1.129	0.692
2.0	9.3	17.8	1.98	0.0235	0.763	0.0421	0.0421	0.142	0.724
2.0	9.3	17.8	2.7	0.0131	0.358	0.0479	0.0500	4.540	0.571
2.0	9.3	17.8	2.7	0.0193	0.481	0.0526	0.0522	–0.651	0.635
2.0	9.3	17.8	2.7	0.0235	0.546	0.0559	0.0535	–4.341	0.661

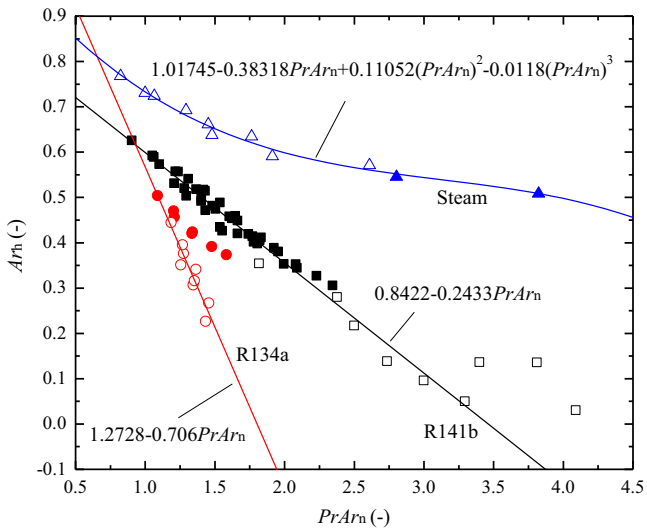

Fig. 4 – Ar_h as the function of $PrAr_n$, (■) R141b (Huang et al., 1999), (□) R141b (Thongtip and Aphornratana, 2015), (●) R134a (Garcia del Valle et al., 2014), (○) R134a (Yan and Cai, 2012), (▲) steam (Eames et al., 1999), (△) steam (Chen and Sun, 1997).

in Section 4.2, all calculated values of Ar_h of two different experimental researches (Huang et al., 1999; Thongtip and Aphornratana, 2015) using R141b locate on one single line as shown in Fig. 4 and can be formulated as Eq. (37).

$$Ar_h = 0.8422 - 0.2433PrAr_n \quad (37)$$

For the working fluid of R134a, two cited experiments yield two inconsistent linear lines in Fig. 4. The inconsistence can be attributed to the different experimental approaches, as one used superheated vapour in experiments to avoid liquid (Garcia del Valle et al., 2014) while the other experiment used saturated vapour and liquid presented during the ejection process (Yan and Cai, 2012), which caused significant changes on fluid density and sound speed as well as the required hypothetical area. The fitting empirical correlation for the case using saturated R134a vapour is given as Eq. (38).

$$Ar_h = 1.2728 - 0.706PrAr_n \quad (38)$$

Due to the involvement of relatively large amount of liquid during the ejection of steam, the relation between Ar_h and $PrAr_n$ is not linear any more as shown in Fig. 4. The fitting empirical correlation is in the form of polynominal as expressed by Eq. (39).

$$Ar_h = 1.01745 - 0.38318PrAr_n + 0.11052(PrAr_n)^2 - 0.0118(PrAr_n)^3 \quad (39)$$

5. Conclusions

The present paper developed a thermodynamic modelling method of ejector used in ejection refrigeration system; and more importantly, the determination method of one of the key but rarely reported parameters has been developed and validated. The primary findings are made as follows:

a) By introducing the experimental results to determine the hypothetical throat area ratio, the present modelling approach reduced the high dependence of modelling accuracy on specifying proper isentropic efficient values. The developed model can predict the critical back pressure (or saturated temperature) with small errors, e.g. less than ±5%.
b) By using the current modelling approach, the values of η_n at 0.93–1.0, η_s at 0.85, and η_d at 0.85 can be adopted for different working fluids and different size ejectors without losing the accuracy of the model; however, the mixing loss factor η_m was varied from 0.95 for nearly pure vapour mixing to 0.67 and 0.72 for the mixing with the appearance of relatively large amount of liquid.
c) For the working fluids of R141b and R134a, the obtained hypothetical throat area ratio Ar_h had linear relationship with the variable $PrAr_n$; when steam was used as working fluid, the developed correlation was in polynominal form due to the involvement of relatively large amount of liquid during the ejection. Using the developed correlations, the model can be employed to predict the ejector performance in critical operation mode. More experimental results are required to further increase the diversity of the working fluid.
d) When liquid-vapour two-phase fluid existed in the ejector, the accuracy of the present model highly relied on the accuracy of calculated two-phase sound speed. Further efforts on selection and verification of two-phase sound speed correlations will be crucial to the ejector performance simulation.

Acknowledgments

The authors gratefully acknowledge the support from the IDRIST project (EP/M008088/1) and Heat-STRESS project (EP/N02155X/1), funded by the Engineering and Physical Sciences Research Council. Data supporting this publication is openly available under an 'Open Data Commons Open Database License'. Additional metadata are available at: http://dx.doi.org/10.17634/152536-1. Please contact Newcastle Research Data Service at rdm@ncl.ac.uk for access instructions.

REFERENCES

Besagni, G., Mereu, R., Inzoli, F., 2016. Ejector refrigeration: a comprehensive review. Renew. Sustain. Energy Rev. 53, 373–403.
Cardemil, J.M., Colle, S., 2012. A general model for evaluation of vapor ejectors performance for application in refrigeration. Energy Convers. Manag. 64, 79–86.
Chen, J., Jarall, S., Havtun, H., Palm, B., 2015. A review on versatile ejector applications in refrigeration systems. Renew. Sustain. Energy Rev. 49, 67–90.
Chen, Y.M., Sun, C.Y., 1997. Experimental study of the performance characteristics of a steam-ejector refrigeration system. Exp. Therm. Fluid Sci. 15, 384–394.
Eames, I.W., Aphornratana, S., Haider, H., 1995. A theoretical and experimental study of a small-scale steam jet refrigerator. Int. J. Refrigeration 18, 378–386.

Eames, I.W., Wu, S., Worall, M., Aphornratana, S., 1999. An experimental investigation of steam ejectors for application in jet-pump refrigerators powered by low-grade heat. Proc. Inst. Mech. Eng. A. J. Power Energy 213, 351–361.
Elbel, S., Lawrence, N., 2016. Review of recent developments in advanced ejector technology. Int. J. Refrigeration 62, 1–18.
Garcia del Valle, J., Saiz Jabardo, J.M., Castro Ruiz, F., San Jose Alonso, J.F., 2014. An experimental investigation of a R134a ejector refrigeration system. Int. J. Refrigeration 46, 105–113.
He, S., Li, Y., Wang, R.Z., 2009. Progress of mathematical modeling on ejectors. Renew. Sustain. Energy Rev. 13, 1760–1780.
Huang, B.J., Chang, J.M., 1999. Empirical correlation for ejector design. Int. J. Refrigeration 22, 379–388.
Huang, B.J., Chang, J.M., Wang, C.P., Petrenko, V.A., 1999. A 1-D analysis of ejector performance. Int. J. Refrigeration 22, 354–364.
Keenan, J.H., Neumann, E.P., 1942. A simple air ejector. J. Appl. Mech. 64, 75–82.
Keenan, J.H., Neumann, E.P., Lustwerk, F., 1950. An investigation of ejector design by analysis and experiment. J. Appl. Mech. 72, 299–309.
Lemmon, E.W., Huber, M.L., McLinden, M.O. NIST reference fluid thermodynamic and transport properties – REFPROP. NIST Standard Reference Database 23 – Version 9.1. 2013.
Li, X., Zhang, Q., Li, X., 2013. A kalian cycle with ejector. Energy 54, 212–219.
Liu, F., Groll, E.A., 2013. Study of ejector efficiencies in refrigeration cycles. Appl. Therm. Eng. 52, 360–370.
Munday, J.T., Bagster, D.F., 1977. A new ejector theory applied to steam jet refrigeration. Ind. Eng. Chem. Process Des. Devel. 16, 442–449.
Nguyen, D.L., Winter, E.R.F., Greiner, M., 1981. Sonic velocity in two-phase systems. Int. J. Multiphase Flow 7, 311–320.
Shestopalov, K.O., Huang, B.J., Petrenko, V.O., Volovyk, O.S., 2015. Investigation of an experimental ejector refrigeration machine operating with refrigerant R245fa at design and off-design working conditions Part 2. Theoretical and experimental results. Int. J. Refrigeration 55, 212–223.
Thongtip, T., Aphornratana, S., 2015. An alternative analysis applied to investigate the ejector performance used in R141b jet-pump refrigeration system. Int. J. Refrigeration 53, 20–33.
Varga, S., Oliveira, A.C., Diaconu, B., 2009. Numerical assessment of steam ejector efficiencies using CFD. Int. J. Refrigeration 32, 1203–1211.
Yan, J., Cai, W., 2012. Area ratio effects to the performance of air-cooled ejector refrigeration cycle with R134a refrigerant. Energy Convers. Manag. 53, 240–246.
Yang, X., Zhang, N., Zhao, L., Deng, S., Li, H., Yu, Z., 2016. Analysis of a novel combined power and ejector-refrigeration cycle. Energy Convers. Manag. 108, 266–274.
Zhu, Y., Cai, W., Wen, C., Li, Y., 2007. Shock circle model for ejector performance evaluation. Energy Convers. Manag. 48, 2533–2541.